Electrochimica Acta 467 (2023) 143003

Contents lists available at ScienceDirect

Electrochimica Acta

journal homepage: www.journals.elsevier.com/electrochimica-acta

Characterization and catalytic prospects of metalloporphyrin-functionalized conducting polymers

Felicia Zaar [a], Rikard Emanuelsson [b], Philipp Gaiser [a], Maria Strømme [a], Martin Sjödin [a,*]

[a] Department of Materials Science and Engineering, Division of Nanotechnology and Functional Materials, Uppsala University, Box 35, SE-751 03 Uppsala, Sweden
[b] Department of Chemistry – BMC, Uppsala University, Box 576, SE-751 23 Uppsala, Sweden

ARTICLE INFO

Keywords:
Conducting polymers
Porphyrins
Electrocatalysis
Redox chemistry
Reaction kinetics

ABSTRACT

Molecular catalysts are attracting interest as drivers of redox reactions for sustainable applications. Through systematic molecular design, they could be engineered to have high selectivity and activity towards a multitude of catalytic reactions. However, as long as they are used in homogeneous setups, they will suffer from inconvenient energy supply, inefficient charge transport and difficulty in separation from reaction products. To be relevant for industrial applications, molecular catalysts must be bound to solid materials in direct contact with the energy source. In this regard, conducting polymers are particularly interesting, as they provide a straightforward means of both surface immobilization and charge transport. In this work, we synthesize and characterize three different metalloporphyrin-functionalized conducting polymers and apply them to catalysis of the hydrogen evolution reaction (HER) and the oxygen reduction reaction (ORR). We show that incorporation of porphyrins into conducting polymers is a reliable immobilization method, that the properties of both the porphyrin units and the polymer backbone are preserved in all systems, and that the polymers provide efficient charge transport to and from the catalytic centers. Nevertheless, we also find that the polymers are negatively affected by intermediates formed during the HER and the ORR. We conclude that the choice of immobilization method has a large impact on the quality of the molecular catalyst, and that the effect of the catalytic cycle on the immobilization matrix must be considered in the molecular design process.

1. Introduction

In connection to the transition towards a more environmentally friendly society, molecular catalysts are attracting interest as parts of sustainable electrocatalytic cycles including e.g. the hydrogen evolution reaction (HER) or oxygen reduction reaction (ORR) for production of fuels and chemicals. Molecular catalysts can be tuned towards high selectivity and activity [1,2] and have proven useful for both electrocatalysis [3,4] and photocatalysis [3,5]. So far, they have mostly been used for homogeneous catalysis, which allows for exact mechanistic resolution, but forces the catalytic process to rely on diffusion for energy supply, requires an excess of catalyst, and makes separation of the reaction products from the catalysts difficult. In addition, homogeneous molecular catalysts must often be activated through redox conversion, meaning that no catalytic activity will be observed until the catalytic molecules have been e.g. reduced. Consequently, the amount of desired product cannot necessarily be increased by simply increasing the driving force of the reaction, as the driving force of substrate conversion will scale only with the reduction potential of the catalyst rather than with the applied potential [6].

In heterogeneous catalysis, the driving force of the catalytic reaction scales with the applied potential (over certain ranges) [7], and both energy supply to the catalytic reaction and separation between the catalyst and reaction products are straightforward. Molecular catalysis would therefore benefit greatly from efficient techniques for surface immobilization, which would produce molecular, heterogeneous catalytic systems. There are already several examples of successful attempts to immobilize molecular catalysts, such as incorporation of Mn(II) complexes into zeolite cages [8], functionalization with organic groups of Si supports [9], various metal-organic frameworks [10] and polymerization of aminophenylporphyrins [11].

An alternative method to immobilize molecular catalysts would be to attach them as pendant groups on a conducting polymer backbone, forming so-called conducting redox polymers (CRPs). A suitable precoursor can be electropolymerized onto various types of current collectors, and offer simple charge transport to the catalytic sites

* Corresponding author.
E-mail address: martin.sjodin@angstrom.uu.se (M. Sjödin).

https://doi.org/10.1016/j.electacta.2023.143003
Received 20 June 2023; Received in revised form 4 August 2023; Accepted 8 August 2023
Available online 9 August 2023

throughout three-dimensional structures. Moreover, the concept is compatible with multiple small molecule pendants. For example, we have previously successfully used CRPs as battery electrode materials [12–14], and for surface immobilization of free base tetraphenylporphyrin [15]. CRPs are thus promising as an immobilization platform for molecular catalysts and redox active small molecules in general. Furthermore, several similar conducting polymer systems have been reported as catalytically active, for example towards the CO_2 reduction reaction [16] and the ORR [17]. However, their versatility in terms of catalytic units and catalytic reactions have not been tested. In addition, it is not known how the polymer network is affected by catalytic cycles or if the catalytic abilities of the active sites are strictly transferrable from homogeneous to heterogeneous conditions.

In this work, we show that immobilization through formation of CRPs can be applied to several metalated tetraphenylporphyrins (MTPP) to produce the alkyldioxythiophene-based polymeric systems pEPE-TPP-M. The same electropolymerization conditions apply to EPE-TPP-M as to the corresponding free base compound, EPE-TPP-H_2, and in some cases, metalation of the free base system is also possible after polymerization. Through a thorough electrochemical characterization, we show that the properties of the polymer and the porphyrin pendants are individually preserved in all systems, and that the conductivity of the polymer improves the reaction kinetics of the porphyrin redox transitions. However, we find that under catalytic conditions, reaction intermediates of the HER and the ORR are harmful to the polymer backbone. We conclude that CRPs are a good platform for surface immobilization of various small molecules, but must be investigated further in catalytic environments before the benefits of conducting polymers can be fully applied to catalysis of the HER and the ORR.

2. Experimental

2.1. General

All commercially available, solid chemicals were purchased from Sigma Aldrich and used as received. Acetonitrile (MeCN, ≥99.5%, AnalaR NORMAPUR® ACS, Reag. pH. Eur. analytical reagent), dichloromethane (DCM, puriss. p.a., ACS reag., reag. ISO, GC, ≥ 99.9%) and dimethylformamide (DMF, ≥99.8%, AnalaR NORMAPUR® ACS, Reag. pH. Eur. analytical reagent) were purchased from VWR chemicals. All electrochemical characterizations were conducted at room temperature in a three-electrode or four-electrode setup using an Autolab PGSTAT032N potentiostat from Metrohm AG equipped with a bipotentiostat module. A Pt wire was used as the counter electrode and 0.1 M tetrabutylammonium hexafluorophosphate ($TBAPF_6$) as the supporting electrolyte. Potentials were measured against an Ag/Ag^+ reference electrode, consisting of an Ag wire in a solution of $AgNO_3$ and electrolyte. In MeCN-based electrolyte $AgNO_3$ was dissolved to 0.01 M and in DCM-based electrolyte to saturation, and in both cases the reference electrode was placed in a separate compartment connected to the bulk solution by a porous frit. The Fc/Fc^+ couple was used as an internal standard, by dissolving a small amount of ferrocene in the electrolyte solution after each round of measurements. Unless otherwise stated, all measurements were performed under N_2 atmosphere, after purging with solvent-saturated N_2.

Glassy carbon (GC) electrodes, Pt wire electrodes and reference electrodes were purchased from Bio-Logic. Glassy carbon electrodes were 3 mm in diameter, 70 mm long and polished with 0.3 μm microalumina powder paste before and after use. Interdigitated array (IDA) electrodes were purchased from Metrohm and consisted of two Au bands, which were 0.75 m long, 150 nm high, 10 μm wide, 10 μm apart and attached to a glass substrate. Indium tin oxide (ITO) glass electrodes were purchased from Praezisions Glas & Optik GmbH.

2.2. Synthesis

EPE-TPP-H_2 was synthesized from EP(OH)E [18] and H_2TPP-COOH as previously reported [15], and then metalated before or after polymerization. To metalate the system before polymerization, EPE-TPP-H_2 (50 mg, 0.045 mmol) was dissolved in DMF (45 mL), resulting in a clear dark red/purple solution. After purging the solution with N_2 for 10 min, the respective metal acetate (10 eq., Co(II)OAc · 4 H_2O, Cu(II)OAc· H_2O or Zn(II)OAc· 2 H_2O) was added and the mixture was stirred at 100 °C for 60–90 min. The reaction was confirmed as complete by thin layer chromatography and the mixture was cooled to room temperature. Water (100 mL) and ethyl acetate (100 mL) were added and the phases were separated. The organic layer was washed with brine (50 mL, saturated solution of NaCl in water) and dried (Na_2SO_4), and the solvent was removed under reduced pressure. Column chromatography (neutral aluminum oxide d = 6 cm, h = 10 cm, CH_2Cl_2/n-pentane: 50%/50% to 100%/0%) yielded the products as red/purple solids. Note that Zn-TPP-COO-EPE was synthesized at half the scale, and that it was precipitated from CH_2Cl_2 by adding MeOH rather than through column chromatography. ^1H nuclear magnetic resonance (NMR) spectra of the products EPE-TPP-Co, EPE-TPP-Cu and EPE-TPP-Zn are available in Figure S1-S3. ^{13}C NMR spectra of EPE-TPP-Cu and EPE-TPP-Zn are shown in Figure S4 and Figure S5, respectively.

Polymerization of both the free base and metallated porphyrin-functionalized trimers (EPE-TPP-X, X = H_2, Co (II), Cu (II), Zn (II)) was performed through potentiodynamic cycling of a solution of 2.5 mM trimer in 0.1 M $TBAPF_6$/DCM, at a scan rate of 0.05 V/s between potential cutoffs −0.7 V and 0.8–1.0 V vs. Fc/Fc^+. The upper cutoff potential was chosen to include any porphyrin redox activity in the potential window (see discussion on polymerization process in Section 3.1). 7–10 cycles in this potential interval window yielded smooth, dark blue/purple films on GC, ITO and IDA electrode surfaces for all EPE-TPP-X. After polymerization, the films were rinsed with acetone to remove any excess electrolyte. Scanning electron microscopy and energy-dispersive X-ray spectroscopy analyses of the film morphology is available for the free base system in ref. [15].

Metalation after polymerization was performed by soaking a polymer-covered electrode in a salt solution containing the metal of interest (5 mM Co(II)OAc · 4 H_2O in DMF, 5 mM Cu(II)OAc · H_2O in DMF or ethanol, 0.1 M $Zn(NO_3)_2$ · 6 H_2O in DMF) overnight. During metalation with Co, the solution was initially heated to 60 °C for 2 h and then to 70 °C for another 2 h, as metalation did not proceed efficiently at either room temperature or 60 °C (see discussion on partial metalation, Section 3.1). The metalation process was further investigated on by recording the UV/vis absorbance spectrum before, during and after soaking of films polymerized onto ITO electrodes. In addition to soaking, metalation with Cu(II) was also achieved through cyclic voltammetry of pEPE-TPP-Cu in 0.1 $TBAPF_6$/MeCN containing 5 mM Cu(II)OAc· H_2O, at a scan rate of 0.1 V/s between approximately −2.3 and 0.6 V vs Fc/Fc^+. After metalation, electrodes were rinsed with acetone to remove any leftover salt from the polymers.

2.3. Cyclic voltammetry

Cyclic voltammograms (CVs) were recorded of the polymers pEPE-TPP-X immobilized onto GC electrodes, in 0.1 M $TBAPF_6$/MeCN at 0.1 V/s. Scan rate studies were conducted for each compound between 0.005 V/s and 1 V/s across all observed redox transitions. CVs of the unpolymerized porphyrin units XTPP were obtained using solutions of 2.5 mM porphyrin in 0.1 M $TBAPF_6$/DCM, and for CoTPP also in 0.1 M $TBAPF_6$/DMF.

2.4. UV/vis spectroscopy

UV/vis spectroscopy was performed using an Agilent 8453 UV–visible single beam spectrophotometer in the interval 190–1100 nm. The

UV/vis absorbance spectra of pEPE-TPP-M (M = Co, Cu, Zn) were obtained by electropolymerizing each trimer onto a translucent ITO electrode under the conditions described in Section 2.2, placing the electrode in a 1 × 1 cm quartz glass cuvette, and subtracting the spectrum of an empty ITO electrode from each sample spectrum. The absorbance spectra of MTPP were obtained by dissolving the porphyrin to 25 μM in DCM in a 1 mm thin layer spectroelectrochemical quartz cell, after subtracting the spectrum of porphyrin-free solution. Spectroelectrochemistry was performed by recording the absorbance every second while simultaneously conducting cyclic voltammetry (0.05 V/s, 0.1 M $TBAPF_6$/MeCN). The change in absorbance (the difference spectrum) was then obtained by subtracting the spectrum recorded at the lower cutoff potential (−1 V vs. Fc/Fc^+) as well as a blank consisting of an empty ITO electrode in electrolyte solution, from all subsequent spectra. In this case, the solution was not purged with N_2.

2.5. Conductance measurements

Each EPE-TPP-M was potentiodynamically electropolymerized onto an Au IDA electrode under the conditions described in Section 2.2, but using bipotentiostatic mode for four-electrode setups at a 0.01 V bias and a cable connector for interdigitated electrodes (Metrohm AG). The conductance of pEPE-TPP-M was then determined by performing bipotentiostatic cyclic voltammetry (0.005 V/s, 0.01 V bias) and measuring the current through the polymer.

2.6. Catalysis

pEPE-TPP-Co immobilized on to GC electrodes was used to catalyze the HER and the ORR in MeCN using the same setup as for cyclic voltammetry. The HER was studied using proton sources of increasing concentration and decreasing pK_a, specifically 0.1 mM, 1 mM, 0.1 M and 1 M acetic acid (AcOH, pK_a 23.5 in MeCN [19]), 1 M p-toluensulfonic acid (PTSA, pK_a 8.5 in MeCN [19]), and 0.1 M and 1 M trifluoromethanesulfonic acid (TfOH, pK_a 0.7 in MeCN [20]). To evaluate the effects of reaction products on the system, a CV of pEPE-TPP-Co was also recorded in H_2-saturated MeCN under H_2 atmosphere. The ORR was studied by purging the electrolyte with O_2 and maintaining an O_2 atmosphere during cyclic voltammetry. The scan rate was set to 0.1 V/s in all cases and the response of an unmodified GC electrode was recorded for reference under the same conditions.

3. Results and discussion

3.1. Metalation

Metalloporphyrin-functionalized CRPs pEPE-TPP-M (M = Co, Cu, Zn) were achieved through post-polymerization metalation of the free base polymeric system pEPE-TPP-H_2, and pre-polymerization metalation of the free base trimeric compound EPE-TPP-H_2. All polymers used and studied in this work are shown in Scheme 1. Unless otherwise stated, the metal centers of the porphyrins are in oxidation state +II.

Pre-polymerization metalation was successful for all investigated pEPE-TPP-M, resulting in high yields (87%, 76% and 98% for M = Co, Cu and Zn, respectively) after minor losses during purification. During cyclic voltammetry of the trimers EPE-TPP-M, an overall and continuous increase in current magnitude was observed for each compound, indicative of oxidative polymerization (see Figure S6). Each polymerization CV also includes 1–3 quasi-reversible redox waves, corresponding to redox transitions of the porphyrin. For EPE-TPP-Cu and EPE-TPP-Zn, the porphyrin transitions are preceded by a nonreversible anodic wave, which is attributed to oxidation of the EPE unit. This wave likely occurs in EPE-TPP-Co as well, but is overlapped by the porphyrin reaction. For all three compounds, efficient polymerization and good reproducibility of polymer properties requires the upper cutoff potential to be set above the potential of the porphyrin redox transitions, suggesting that the EPE unit needs to be oxidized twice for efficient polymerization to occur. These results are in good agreement with those obtained for the free base compound EPE-TPP-H_2 [15]. However, the onset of polymerization is approximately 0 V vs. Fc/Fc^+ for all three metalated compounds, which is lower than the 0.3 V onset observed for the free base system.

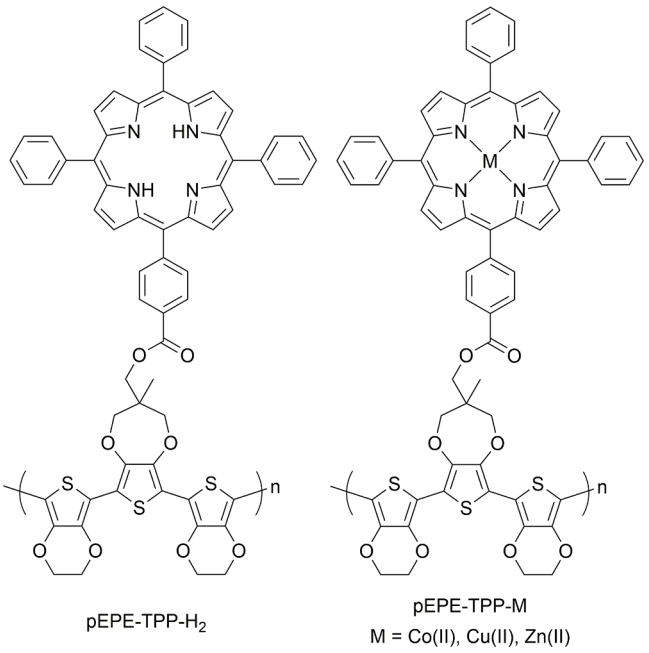

Scheme 1. Polymeric systems used and studied in this work.

Post-polymerization metalation was less complete than pre-polymerization metalation for pEPE-TPP-Co. For pre-metalated pEPE-TPP-Co, the half-wave potentials of the porphyrin redox transitions (discussed in detail in Section 3.2.1.) are in good agreement with the half-wave potentials of CoTPP in solution, and in much better agreement than with the half-wave potentials of H_2TPP in solution. For post-metalated pEPE-TPP-Co, the half-wave potentials are only partially shifted from those of the free base towards those of CoTPP. That the metalation is only partial is also clear from UV/vis spectroscopy (see Figure S7a), where features associated with H_2TPP only partially change towards those associated with CoTPP throughout the metalation process. It should be noted that the half-wave potentials of pEPE-TPP-Co agree with those of CoTPP measured in DMF, but not with those of CoTPP measured in DCM. It is likely that the redox transition of the metal center (Co(III)/Co(II)) is sensitive to the polarity of the surrounding environment, and that the charged polymer is more similar to the more polar solvent DMF than the less polar solvent DCM.

For pEPE-TPP-Cu, post-polymerization metalation works well in terms of reproducibility and correspondence of porphyrin half-wave potentials with those of CuTPP. UV/vis spectra of the metalation process, as well as the results of cycling pEPE-TPP-Cu in the presence of Cu(II)OAc · H_2O, suggest that a larger portion of the porphyrins than for pEPE-TPP-Co becomes metalated (see Figure S7b and S8). In fact, the difference in half-wave potentials is smaller between post-metalated pEPE-TPP-Cu and CuTPP than between pre-metalated pEPE-TPP-Cu and CuTPP. However, pre-metalated films display a more reversible porphyrin response at low potentials (where the polymer is not conducting), and a larger porphyrin response at high potentials (where the polymer is conducting), than post-metalated films. In other words, the redox chemistry of the pre-metalated pEPE-TPP-Cu films is more distinct from that of the free base system than the post-metalated pEPE-TPP-Cu films. The same type of behavior is observed for pEPE-TPP-Co, which clearly undergoes only partial metalation after polymerization. Thus, post-polymerization metalation with Cu(II) is not complete, but may be more efficient than post-polymerization with Co(II). For pEPE-TPP-Zn,

both cyclic voltammetry and UV/vis spectroscopy suggest that post-polymerization metalation results in a fully metalated system that is essentially identical to the pre-metalated one.

It has previously been suggested that the degree of post-polymerization metalation for Mg and Co polyporphine films depends on the film thickness [21]. However, the results of our study suggest that the most important factor for successful post-polymerization metalation is the packing of the porphyrins. As will be discussed in Sections 3.2.3. and 3.4, ZnTPP and H_2TPP seem to π-stack, whereas CoTPP and CuTPP do not. A likely explanation is that five- or six-coordination is favorable for Co(II) and Cu(II) in tetraphenylporphyrins, in which case axial ligands would increase the shortest possible distance between porphyrin units, particularly if the axial ligand bonds are lengthened by Jahn-Teller distortion. As a result, Co(II) and Cu(II) would have difficulty adjusting to the tightly packed, planar porphyrin units in pEPE-TPP-H_2, leaving metalation partial. Zn(II), on the other hand, may prefer four-coordination to the porphyrin ligand and thereby be able to completely metalate pEPE-TPP-H_2. A summary of post-and pre--polymerization electrochemical behavior is available in Fig. 1 and in Scheme S1.

3.2. Electrochemical characterization

3.2.1. Redox activity

pEPE-TPP-Co, pEPE-TPP-Cu and pEPE-TPP-Zn all undergo oxidative polymer doping, i.e. continuous oxidation of the many overlapping redox sates of the polymer chains [22,23]. This is indicated by the increase in current magnitude beginning around −0.6 V vs. Fc/Fc$^+$, and means that the polymer backbones are able to transport charge as expected. In this regard, the metalated systems all behave like the free base system [15].

All investigated pEPE-TPP-X systems are also quasi-reversibly redox active, displaying 1–2 oxidative transitions and 1–2 reductive transitions in relation to their open circuit potentials of approximately −0.3 V vs. Fc/Fc$^+$ (the CVs of H_2TPP and pEPE-TPP-H_2 are available in Figure S9). These redox transitions occur either at the porphyrin ligand or at the metal center, and will be referred to as L^m/L^n for changes from ligand charge m to ligand charge n, or as M(p)/M(q) for changes from metal oxidation state p to metal oxidation state q. The formal potential of each redox transition is here approximated as the half-wave potential, determined by taking the average of the anodic and cathodic peak potentials associated with the reaction. The approximation should be accurate, as all redox conversions discussed here are at least quasi-reversible and the diffusion coefficients are not expected to vary notably between oxidized and reduced species of a given reaction.

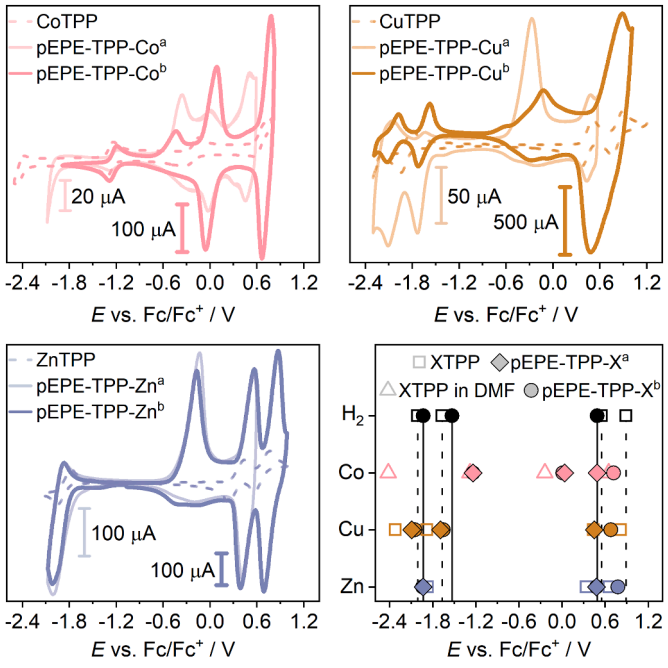

Fig. 1. CVs of pEPE-TPP-M (0.1 V/s, 0.1 M TBAPF$_6$/MeCN) and the corresponding MTPP (0.1 V/s, 0.1 M TBAPF$_6$/DCM for M = Cu, Zn, 0.1 M TBAPF$_6$/DMF for M = Co). A summary of the half-wave potentials is shown to the bottom right, where the free base is included for reference. [a]Metalation after polymerization. [b]Metalation before polymerization.

pEPE-TPP-Co undergoes three redox transitions, and according to studies of CoTPP in solution [24–31], these correspond to the Co(II)/Co(I), Co(III)/Co(II) and $L^{1+/0}$ transitions. For pre-metalated pEPE-TPP-Co, they occur at −1.24, 0.01 and 0.72 V vs. Fc/Fc$^+$, respectively. The first and last agree well with the half-wave potentials of CoTPP in solution, whereas the Co(III)/Co(II) transition in pEPE-TPP-Co occurs approximately 0.2 V positive of the corresponding transition in CoTPP dissolved in DMF (see Table 1). For post-metalated pEPE-TPP-Co, only the half-wave potential of the Co(II)/Co(I) transition agrees with that of CoTPP. The half-wave potential of the $L^{1+/0}$ transition in post-metalated pEPE-TPP-Co is identical to that of pEPE-TPP-H_2, indicating partial metalation.

pEPE-TPP-Cu displays the $L^{1-/2-}$, $L^{0/1-}$ and $L^{1+/0}$ transitions, according to studies of CuTPP in solution [24,25,27,29,30,32–34]. For pre-metalated pEPE-TPP-Cu, these occur at −2.05, −1.65 and 0.68 V vs. Fc/Fc$^+$, respectively, and for post-metalated pEPE-TPP-Cu at −2.09, −1.69 and 0.45 V vs. Fc/Fc$^+$, respectively. The $L^{1-/2-}$ and $L^{0/1-}$ transitions occur at more negative potentials for pEPE-TPP-Cu than for pEPE-TPP-H_2, just like the $L^{1-/2-}$ and $L^{0/1-}$ transitions occur at more negative potentials for CuTPP than for H_2TPP in solution. The $L^{1+/0}$ transition, however, occurs at almost the same potential for post-metalated pEPE-TPP-Cu and pEPE-TPP-H_2, but at a higher potential for pre-metalated pEPE-TPP-Cu than for pEPE-TPP-H_2. For pre-metalated pEPE-TPP-Cu, the $L^{1+/0}$ transition occurs at 0.68 V vs. Fc/Fc$^+$, which is close to the average of the half-wave potentials of the $L^{1+/0}$ and $L^{2+/1+}$ transitions for CuTPP in solution. The similarities in redox chemistry between post-metalated pEPE-TPP-Cu and pEPE-TPP-H_2, as well as the differences in redox behavior between pre-

Table 1
Redox chemistry of XTPP in solution (V vs. Fc/Fc$^+$, 0.1 V/s, 0.1 M TBAPF$_6$/DCM or 0.1 M TBAPF$_6$/DMF) and of surface-immobilized pEPE-TPP-X (V vs. Fc/Fc$^+$, 0.1 V/s, 0.1 M TBAPF$_6$/MeCN).

Compound	L^{1-}/L^{2-}	L^0/L^{1-}	M(II)/M (I)	M(III)/M (II)	L^{1+}/L^0	L^{2+}/L^{1+}
H_2TPP[a]	−1.99	−1.64			0.56	0.90
pEPE-TPP-H_2[a]	−1.93	−1.53			0.49	
CoTPP in DCM		−1.91	−1.39	0.34	0.55	0.79
CoTPP in DMF		−2.42	−1.27	−0.19	0.64	
pEPE-TPP-Co[b]			−1.24	0.01	0.72	
pEPE-TPP-Co[c]			−1.24	0.04	0.49	
CuTPP[a]	−2.32	−1.88			0.44	0.82
pEPE-TPP-Cu[b]	−2.05	−1.65			0.68	
pEPE-TPP-Cu[c]	−2.09	−1.69			0.45	
ZnTPP[a]		−1.85			0.36	0.66
pEPE-TPP-Zn[b]		−1.94			0.48	0.78
pEPE-TPP-Zn[c]		−1.93			0.48	

[a] Previously reported in ref. [15].
[b] Pre-polymerization metalation.
[c] Post-polymerization metalation.

and post-metalated pEPE-TPP-Cu, suggest that post-polymerization metalation is only partial for this system.

pEPE-TPP-Zn undergoes the $L^{1-/2-}$, $L^{0/1-}$ and $L^{1+/0}$ transitions, by comparison with studies of ZnTPP in solution [24,25,27,28,30,33,35–38]. These reactions occur at the same, or almost the same, potentials for pre- and post-metalated pEPE-TPP-Zn, indicating complete post-polymerization metalation. Like the $L^{0/1-}$ occurs at more negative potentials for ZnTPP than for H_2TPP, it occurs at more negative potentials for pEPE-TPP-Zn than for pEPE-TPP-H_2. However, the $L^{1+/0}$ occurs at about the same potential in pEPE-TPP-Zn as in pEPE-TPP-H_2, despite this transition occurring at substantially less positive potentials for ZnTPP than for H_2TPP.

A summary of the half-wave potentials of all observed redox transitions is shown in Table 1 and Table S1. In general, the agreement in porphyrin half-wave potentials between the polymeric and solvated systems is higher for the porphyrin reductions than for the oxidations. This discrepancy is in part due to interactions between the porphyrin redox activity and the doping of the polymer backbone at oxidative potentials. As will be discussed below, the choice of metal center in the porphyrins has a clear influence on the behavior on the doping profile and conductance of the polymer. However, the redox chemistry of both XTPP in solution and pEPE-TPP-X will also be affected by the local environment. Differences in polarity between the polymer matrix and the pure solvent (as well as between DCM, DMF and MeCN), variations in the formation of solvent cages, and interactions between porphyrins or between the linker and the polymer backbone may all affect the half-wave potentials. Thus, immobilization of porphyrins into CRP films affords qualitatively the same but not identical redox chemistry to porphyrins in solution.

3.2.2. Charge balance

In the potential region where the polymer is not conducting, the reductive porphyrin redox peaks are larger than their oxidative counterparts for all systems. For all systems, there is also an anodic peak at the onset of polymer doping, which becomes substantially less pronounced if these redox transitions are not included in the scan. These effects result from charge trapping during porphyrin reduction at low potentials [15]. The amount of charge passed during reduction and oxidation of the system can be calculated by integrating and comparing the anodic and cathodic current responses within the potential region of interest. For example, 858 μC is passed between −1.1 and −2.1 V vs. Fc/Fc^+ during reduction from L^0 to L^{1-} in pEPE-TPP-Zn. During reoxidation over the same potential region, only 144 mC is passed, resulting in a difference in charge between reduction and oxidation of 714 μC. However, if the potential region is extended to include the anodic peak at the onset of polymer doping (−2.1 to 0.2 V vs. Fc/Fc^+), the charge difference is only 269 μC, and thereafter decreases further. This implies that the charges trapped during reduction of the porphyrin units in the potential region where the polymer is not conducting, are to a large extent released as soon as the polymer becomes conducting, and that the remaining trapped charges are released as the degree of polymer doping is increased. The amount of charge trapping varies between the systems and is likely determined by a combination of polymer packing, interaction between the porphyrins and the polymer backbone, and film thickness. More information can be found in Figure S10 and Table S2.

By calculating the charges passed across a porphyrin redox peak in the potential region where the polymer is conducting, and comparing it to the accumulated polymer response throughout this potential region, the doping level of the polymer backbone can be estimated (see Figure S11). As summarized in Table S3, the ratio between porphyrin and polymer charges is about 1/2 for all pre-metalated systems. Given that there is one porphyrin per trimer unit and assuming that all porphyrin units are accessed at high potentials (which is reasonable according to the small peak splits observed in the scan rate studies described below), about 1 in every 6 thiophene subunits of the polymer chains become oxidized in the potential windows studied here.

3.2.3. Reaction kinetics and limitations

Scan rate studies were conducted to evaluate the influence of the charge transport abilities of the polymer backbone on the kinetics and limitations of the porphyrin redox conversions. For a system that is not limited by diffusion, such as a Nernstian redox reaction occurring in a surface bound system, the peak current of the reduction (or oxidation) wave increases linearly with the scan rate v if the entire material is redox converted [39]:

$$\left|i_{p,red}\right| = \frac{z^2F^2A\Gamma_{ox}}{4RT}v \tag{1}$$

where z is the number of charges transferred in the reaction, F is the Faraday constant, A is the area of the electrode, Γ_{ox} is the surface coverage of the oxidized species, R is the gas constant and T is the temperature (the equation also applies if $i_{p,red}$ is replaced by $i_{p,ox}$ and Γ_{ox} by Γ_{red}). Equivalently, the logarithm of the peak current is proportional to the logarithm of the scan rate with unity slope:

$$\ln\left(\left|i_{p,red}\right|\right) \propto c_1 + \ln v \tag{2}$$

where c_1 is a constant. For a reaction governed by linear diffusion, the peak current is instead proportional to the square root of the scan rate [40]:

$$\left|i_{p,red}\right| = 0.4463AC^*_{ox}\left(\frac{z^3F^3D_{ox}}{RT}\right)^{1/2}v^{1/2} \tag{3}$$

Here, C^*_{ox} is the bulk concentration of the oxidized species and D_{ox} is the diffusion coefficient of the oxidized species. Equation (3) is equivalent to

$$\ln\left(\left|i_{p,red}\right|\right) \propto c_2 + 0.5\ln v \tag{4}$$

where c_2 is another constant.

In addition to the peak current, the scan rate also affects the potential difference between the oxidation and reduction peaks. For a Nernstian, surface bound system $\Delta E_p = E_{p,red} - E_{p,ox} = 0\ V$ [39], and for a system governed by linear diffusion at room temperature, $\Delta E_p = 57/z$ mV [40]. These relations hold in ideal systems, free from solution resistance, convection, side reactions and other interferences. They are also only true at scan rates low enough that the reaction kinetics are much faster than the change in potential. Thus, the higher the scan rate at which ΔE_p diverges from ideality, the faster the redox reaction.

Figure 2 shows $\ln(|i_{p,red}|)$ and ΔE_p as functions of $\ln(v)$ for the pre-metalated systems. The redox transitions of pEPE-TPP-Co and pEPE-TPP-Cu occurring at low potentials (here denoted I^-/II^- and $0/I^-$ to include both ligand- and metal-centered reactions) have slopes that are exactly or close to 0.5 throughout the full scan rate interval 0.005–1 V/s. In addition, $\Delta E_p > 57$ mV for all scan rates. These results clearly indicate that the Co(II)/Co(I) transition of pEPE-TPP-Co and the L^{1-}/L^{2-} transition of pEPE-TPP-Cu are governed by diffusion, and that redox conversion throughout the film is incomplete (the scan rate study of the L^0/L^{1-} transition in pEPE-TPP-Zn did not yield any useful results due to poor reversibility). It should be noted that the L^0/L^{1-} transition of pEPE-TPP-Cu is not visible unless the potential region where the polymer is doped is included in the scan. This can be explained by the difference in polymer packing between the doped and undoped states of the polymer. During doping, the polymer swells due to intercalation of counter ions, facilitating ion transport through the film. Dedoping then causes the counter ions to be expelled, the polymer to contract and the ion transport to be impeded. Poor ion transport can, in turn, intensify irreversibility and charge trapping during redox activity. This is evident from Figure S12, which shows the first scan rate measurement of pEPE-TPP-Cu at low potentials. In the first cycle, both the L^0/L^{1-} and the L^{1-}/L^{2-} reductions are visible, but only the L^{1-}/L^0 reoxidation. In the second cycle, only the L^{1-}/L^{2-} transition occurs. This suggests that as the polymer contracts, charges are trapped within it such that the L^0 state can no longer be reached, leaving only the L^{1-}/L^{2-} transition for the following scan rate measurements.

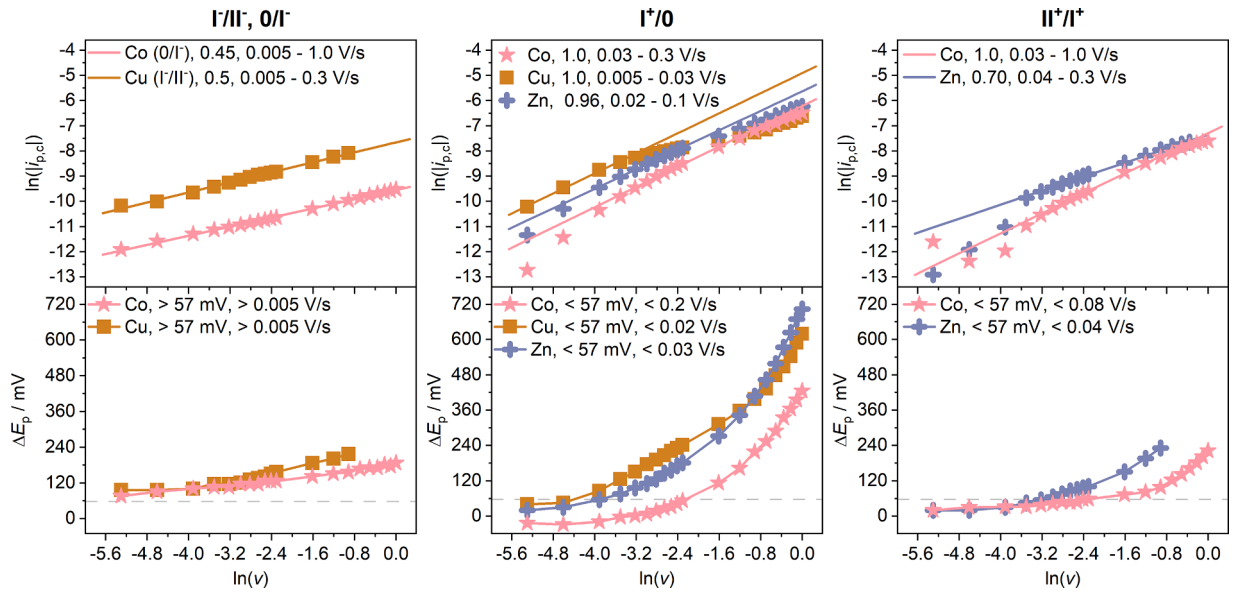

Fig. 2. $\ln(|i_{p,red}|)$ and ΔE_p as functions of $\ln(\nu)$ for pEPE-TPP-M (0.005–1.0 V/s, 0.1 M $TBAPF_6$/MeCN). In the upper panels, labels show M, the slope of the linear fit, and the scan rate interval in which this linear fit applies. In the lower panels, the labels show M, if the peak separation is larger or smaller than 57 mV, and in which scan rate interval this relation applies.

From Fig. 2, it is clear that at high potentials, pEPE-TPP-Co, pEPE-TPP-Cu and pEPE-TPP-Zn all behave like surface bound systems. The slope of the $I^+/0$ transition (referring to either M(III)/M(II) or L^{1+}/L^0) is exactly or close to unity between 0.03 and 0.3 V/s, 0.005 and 0.03 V/s, and 0.02 and 0.1 V/s for pEPE-TPP-Co, pEPE-TPP-Cu and pEPE-TPP-Zn, respectively. In addition, $\Delta E_p < 57$ mV at low scan rates for all three systems. For pEPE-TPP-Co, $\Delta E_p < 57$ mV all the way up to 0.2 V/s, indicating this system can be completely (or almost completely) redox converted with high efficiency. Redox conversion is also complete in the lower section of the scan rate interval during the II^+/I^+ transition in pEPE-TPP-Co and pEPE-TPP-Zn. All CVs related to the scan rate studies in MeCN are available in Figure S13-S15.

For pre-metalated pEPE-TPP-Co and pEPE-TPP-Cu, the difference in redox behavior between high and low potentials (surface-like vs. diffusion-limited) can be related to the heights of the redox peaks. For these systems, the porphyrin transitions at low potentials are notably smaller than the porphyrin transitions at high potentials. This can be explained by the ease of diffusion through the film, supported by the observation that the porphyrin peaks at low potentials are less affected by film thickness than the transitions at high potentials (see Figure S16). At high potentials, where the polymer is conducting, the full film can be accessed and the magnitude of the porphyrin response will scale with the number of porphyrins in the film. At low potentials, where redox conversion relies on diffusion, it is likely that redox conversion only happens in the porphyrins closest to the electrode surface (or at the polymer-solvent interface, depending on whether electron or ion transport is limiting), i.e. the number of porphyrins that are reached at low potentials depends on the extent of the diffusion gradient into the film. The gradient is determined by the diffusivity if the charged species involved in the reaction rather than the thickness of the film, meaning that the height of the porphyrin redox peaks at low potentials should not be strongly affected by film thickness. However, the dense packing of the porphyrin matrix at low potentials impedes ion transport, which may be more noticeable in a thick film. This may result in slightly smaller diffusion-limited redox peaks in a thick film than in a thin one, an effect that is exemplified by pEPE-TPP-Co in Figure S16.

For pEPE-TPP-Zn, post-metalated pEPE-TPP-Cu and pEPE-TPP-H_2, there is no obvious relation between peak height, system limitations and film thickness. For pEPE-TPP-Zn, the porphyrin transitions give rise to peaks that are about the same height throughout the entire potential window and for post-metalated pEPE-TPP-Cu and pEPE-TPP-H_2 the peaks at low potentials are higher than the peaks at high potentials. These behaviors cannot be explained by ease of diffusion through the film, but may instead be an issue of porphyrin stacking. In pEPE-TPP-H_2, the porphyrin units are planar and likely to π-stack, and it has been shown that a large portion of the charge transport of this system originates in hopping through the porphyrins [15]. This charge transport may compete with that of the polymer backbone, such that the baseline for the porphyrin transitions at high potentials occurs within the current response of the polymer. Given that post-metalated pEPE-TPP-Cu is only partially metalated, its current response can be expected to be similar to that of pEPE-TPP-H_2. As will be shown in Section 3.4, the conductance profile of pEPE-TPP-Zn is more similar to that of pEPE-TPP-H_2 than to that of pre-metalated pEPE-TPP-Co and pEPE-TPP-Cu, indicating that ZnTPP are able to π-stack whereas CoTPP and CuTPP are not, presumably due to a difference in coordination geometries.

3.3. Spectroelectrochemistry

To ensure that the porphyrin and polymer features of the metalated systems can be individually accessed, pEPE-TPP-Co was investigated with spectroelectrochemistry. Figure 3a shows the change in UV/vis absorbance as pEPE-TPP-Co is oxidized through polymer doping and the Co(III)/Co(II) and L^{1+}/L^0 transitions of the porphyrin. Similarly to what was observed for the free base system [15], the spectra include features related to both the polymer backbone and the porphyrin units. The porphyrin features include the Soret band, a single Q band and a wide band at short wavelengths (see Figure S17c). Changes to the Soret band can be seen at 394 and 438 nm, changes to the Q band at 528 and 546 nm, and to the wide absorption band at 326 and 353 nm. The changes in absorbance associated with the polymer backbone occur due to a decrease of bandgap transitions at and around 617 nm, and an increase of polaron/bipolaron transitions at and around 895 nm.

The fact that each of the porphyrin features changes at two distinct wavelengths indicates that the porphyrin units undergo two successful, separate oxidations. Indeed, if the absorbance at each wavelength associated with a change in the spectrum is plotted against potential, it is clear that the polymer doping and the two porphyrin oxidations occur as independent events. This is shown in Fig. 3b, where the changes to the polymer features (blue lines) begin at the onset of polymer doping, the

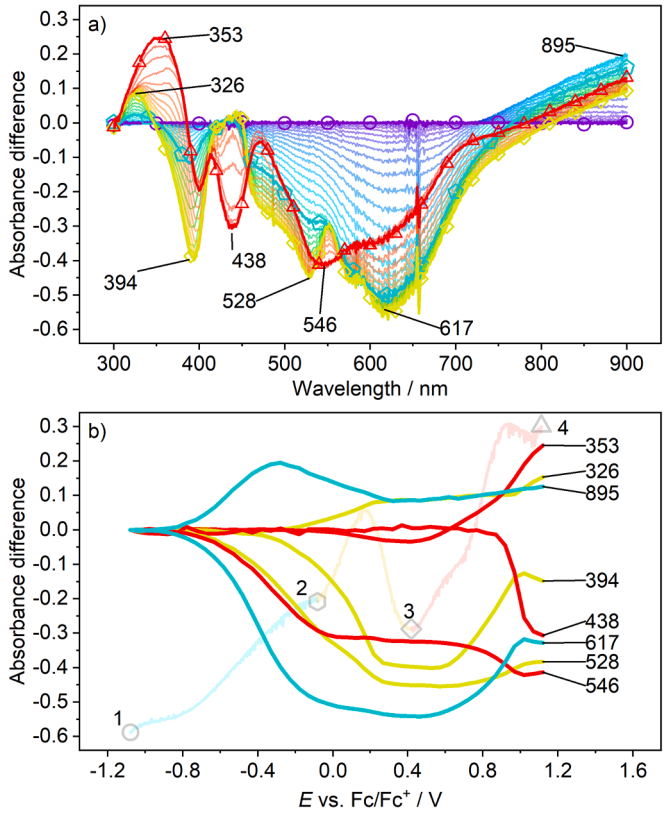

Fig. 3. a) Difference spectrum of pEPE-TPP-Co during oxidation of the polymer backbone and the porphyrin units. Changes to the porphyrin features occur at 326, 353, 394, 438, 528 and 546 nm, and changes to polymer features at 617 and 895 nm. The absorbances highlighted by symbols and color correspond to potentials 1–4 marked in b). b) Changes in polymer and porphyrin spectroscopic features with potential. The numbers to the right show the wavelengths at which the features occur in the difference spectrum, the faded lines in the background show the forward scan of the corresponding CV, and the symbols 1–4 indicate the starting potential, the onset of the Co(III)/Co(II) transition, the onset of the L^{1+}/L^{0} transition and the end potential, respectively.

first set of changes to the porphyrin features (green lines) at the potential of the Co(III)/Co(II) transition, and the second set of changes to the porphyrin features (red lines) at the potential of the L^{1+}/L^{0} transition (though it should be noted that the independence between polymer and porphyrin is slightly less clear for the features at 528 and 546 nm, as these overlap with the wavelengths of the polymer bandgap). These observations confirm that the properties of the two building-blocks of the system – the conductivity of the polymer and the redox activity of the porphyrins – are individually preserved in pEPE-TPP-Co. As this behavior is identical to that of the free base system [15], it was also assumed to apply to pEPE-TPP-Cu and pEPE-TPP-Zn.

3.4. Conductance measurements

The conductance of pEPE-TPP-Co, pEPE-TPP-Cu and pEPE-TPP-Zn was investigated in order to evaluate the efficiency of charge transport through the polymer backbone and the porphyrin units. Each trimer was polymerized onto an IDA electrode, which consists of two closely spaced Au working electrodes, WE1 and WE2. By applying a potential bias across WE1 and WE2 and performing cyclic voltammetry using both electrodes simultaneously, a current will flow through the polymer once it becomes conducting during doping. Provided that this current is much larger than the faradaic contributions to the total current, the conductance across the polymer is given by [41]:

$$G_{\mathrm{pol}} = \frac{\Delta i}{2E_{\mathrm{bias}}} \tag{5}$$

where Δi is the difference between the currents measured on the two working electrodes, and E_{bias} is the voltage bias applied across them (see Section 3.3 of the Supporting Information for details).

As shown in Fig. 4, pEPE-TPP-Co and pEPE-TPP-Cu undergo a strong increase in conductance beginning at approximately the same potential as the onset of doping. However, in contrast to the free base system [15], the conductance does not increase during porphyrin oxidation and reduction, indicating that there is no contribution to the charge transport through hopping via the porphyrin units (the small changes in conductance at the potentials of the porphyrin transitions result from differences in the measured faradaic contributions between WE1 and WE2). pEPE-TPP-Zn, on the other hand, has a conductance profile similar to that of pEPE-TPP-H_2, in that there is a strong increase in conductance at the potential of the porphyrin conversion, in addition to that at the onset of polymer doping. This indicates that in pEPE-TPP-Zn, charges are transported not only through the polymer backbone, but also through the porphyrin units. Taken together, these observations are in agreement with the argument that CoTPP and CuTPP have different coordination geometries from ZnTPP and H_2TPP, resulting in that CoTPP and CuTPP are not able to π-stack to the same extent as ZnTPP and H_2TPP and that charge transport via the porphyrins is prevented in pEPE-TPP-Co and pEPE-TPP-Cu.

3.5. Catalysis

To evaluate the influence of the polymer backbone on the efficiency of catalysis, pEPE-TPP-Co was used to catalyze the HER in the presence of increasing concentrations of acid, and acids with decreasing pK_a. Figure 5a shows CVs of pEPE-TPP-Co in the presence of 0.1 mM - 1 M AcOH, 1 M PTSA and 50 mM - 0.5 M TfOH. A catalytic wave is observed in all cases, and occurs at less and less negative potentials throughout the series. In the presence of 0.5 M TfOH, the catalytic wave occurs within the potential region where the polymer is conducting. However, here the catalytic reaction has a detrimental effect on the polymer backbone, and the porphyrin response disappears. One possible explanation could have been that the polymer was directly affected by the strongly acidic environment, but as shown in Fig. 5b, the current response does not dramatically change until the catalytic reaction is included in the potential window of the scan.

Figure 5c shows cycling of pEPE-TPP-Co under H_2 atmosphere, in H_2-saturated MeCN. The upper cutoff potential is gradually increased past the potential of the HER in the presence of 0.5 TfOH, to finally reach the full stability window of the polymer. It is evident that H_2, i.e. the reaction product of the HER, is not harmful to the system. Rather, it is likely that e.g. an H radical species, formed as an intermediate in the catalytic cycle, attacks the double bonds throughout the polymer and destroys the polymer π-network.

To further evaluate the effects on polymeric systems of reaction products and intermediates formed during a catalytic cycle, pEPE-TPP-Co was also used to catalyze the ORR in O_2-saturated MeCN under O_2 atmosphere. In Figure S20a, a small catalytic current can be seen at the potential of the Co(II)/Co(I) transition. However, the polymer gradually degrades until its current response strongly resembles that of an empty GC electrode. For GC, the response is not catalytic, but reversible. Given the lack of water and protons in the solution, it is likely that GC simply converts O_2 back and forth between its neutral and radical species. The response of pEPE-TPP-Co also dramatically changes even if the upper potential cutoff is set below the onset of polymer doping (see Figure S20b). The Co(II)/Co(I) peak gradually changes into the GC response, but in this case the polymer remains more intact. It thus appears that O_2 or a biproduct of the ORR attacks the ester linkers between the porphyrins and the trimer units, and that the swelling of the polymer

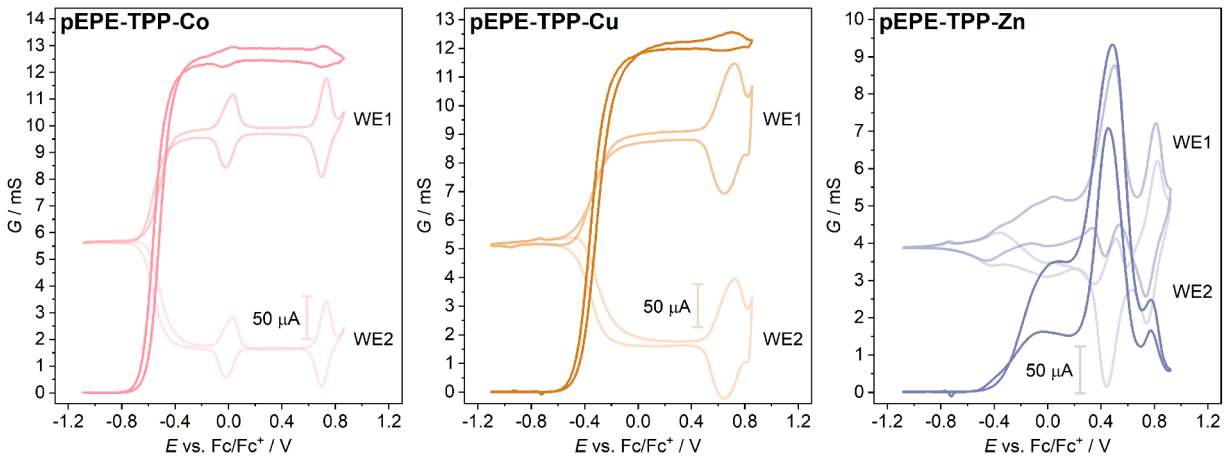

Fig. 4. Conductance of pEPE-TPP-Co, pEPE-TPP-Cu and pEPE-TPP-Zn (0.005 V/s, 0.1 M $TBAPF_6$/MeCN). The corresponding CVs recorded on WE1 and WE2 are shown in the background.

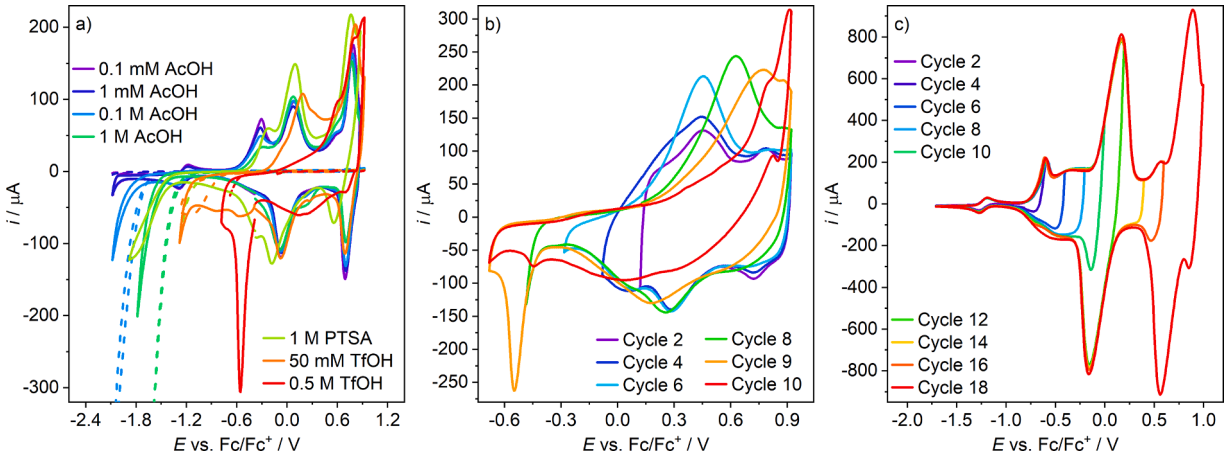

Fig. 5. a) Catalysis of the HER by pEPE-TPP-Co using acids at increasing concentration and with decreasing pK_a. GC response (dashed lines) included for reference. b) Cycling of pEPE-TPP-Co using decreasing lower cutoff potential. c) Cycling of pEPE-TPP-Co in the presence of H_2 using increasing upper cutoff potential.

that occurs during doping enhances this process by facilitating diffusion of the harmful species to the attack sites. These results suggest that pEPE-TPP-Co is unsuitable for catalysis of the ORR until the degradation mechanism has been better understood and counteracted, but also that CoTPP may be able catalyze electrochemical cleavage of ester bonds, which is interesting for chemical synthesis.

As tetraphenylporphyrins and other similar structures have previously been used successfully towards both the HER [42–44] and the ORR [45,21, 46–48] in homogeneous setups it is clear that the choice of immobilization method has a large impact on the quality of molecular catalysis. It is not necessarily the case that the catalytic behavior of a molecule is transferrable from a homogenous to a heterogenous environment, unless the impact of the catalytic cycle on the immobilization matrix is accounted for.

4. Conclusion

We have synthesized and characterized three systems for molecular electrocatalysis consisting of metalloporphyrin-functionalized conducting polymers. The same polymerization conditions apply to all three metalated systems as to the corresponding free base system. Metalation of the free base system is possible before and after polymerization, but in particular for the pEPE-TPP-Co and pEPE-TPP-Cu, pre-polymerization metalation is more complete than post-polymerization metalation. The properties of the porphyrins as well as of the polymer backbones are individually preserved in all systems, and the polymer facilitates charge transport to and from the porphyrin redox centers. These qualities make the systems promising for molecular, heterogeneous catalysis. However, during both the HER and the ORR, the polymer backbone is negatively affected by some reaction intermediate. In conclusion, CRPs can be used as a platform for straightforward immobilization of redox active metalloporphyrins, but successful catalysis by molecular catalysts incorporated into polymeric systems requires better understanding of the effects of the catalytic cycle on the polymer matrix. Studies aimed at identifying the harmful intermediates of the HER and the ORR are ongoing.

CRediT authorship contribution statement

Felicia Zaar: Methodology, Formal analysis, Investigation, Writing – original draft, Visualization. **Rikard Emanuelsson:** Conceptualization, Writing – review & editing, Supervision. **Philipp Gaiser:** Methodology, Investigation, Writing – review & editing. **Maria Strømme:** Resources, Writing – review & editing, Funding acquisition. **Martin Sjödin:** Conceptualization, Methodology, Resources, Writing – review & editing, Supervision, Funding acquisition.

Declaration of Competing Interest

The authors declare that they have no known competing financial interests or personal relationships that could have appeared to influence the work reported in this paper.

Data availability

Data will be made available on request.

Acknowledgments

This study was funded by Formas – a Swedish Research Council for Sustainable Development (grant number: 2019-01285), the Åforsk foundation (19-352). It made use of the NMR Uppsala infrastructure, which is funded by the Department of Chemistry-BMC and the Disciplinary Domain of Medicine and Pharmacy.

Supplementary materials

Supplementary material associated with this article can be found, in the online version, at doi:10.1016/j.electacta.2023.143003.

References

[1] C. Cometto, L. Chen, P.K. Lo, Z. Guo, K.C. Lau, E. Anxolabéhère-Mallart, C. Fave, T. C. Lau, M. Robert, Highly selective molecular catalysts for the CO2-to-CO electrochemical conversion at very low overpotential. contrasting Fe vs Co quaterpyridine complexes upon mechanistic studies, ACS Catal. 8 (2018) 3411–3417, https://doi.org/10.1021/acscatal.7b04412.

[2] A. Corma, H. Garcia, Crossing the borders between homogeneous and heterogeneous catalysis: developing recoverable and reusable catalytic systems, Top. Catal. 48 (2008) 8–31, https://doi.org/10.1007/s11244-008-9056-5.

[3] W. Zhang, W. Lai, R. Cao, Energy-related small molecule activation reactions: oxygen reduction and hydrogen and oxygen evolution reactions catalyzed by porphyrin-and corrole-based systems, Chem. Rev. 117 (2017) 3717–3797, https://doi.org/10.1021/acs.chemrev.6b00299.

[4] N. Kaeffer, W. Leitner, Electrocatalysis with molecular transition-metal complexes for reductive organic synthesis, J. Am. Chem. Soc. 2 (2022) 1266–1289, https://doi.org/10.1021/jacsau.2c00031.

[5] M.V. Bobo, J.J. Kuchta, A.K. Vannucci, Recent advancements in the development of molecular organic photocatalysts, Org. Biomol. Chem. 19 (2021) 4816–4834, https://doi.org/10.1039/d1ob00396h.

[6] M. Jackson, C. Kaminsky, S. Oh, J. Melville, Y. Surendranath, Graphite conjugation eliminates redox intermediates in molecular electrocatalysis, J. Am. Chem. Soc. 141 (2019) 14160–14167, https://doi.org/10.1021/jacs.9b04981.

[7] A. Appel, M. Helm, Determining the overpotential for a molecular electrocatalyst, ACS Catal. 4 (2014) 630–633, https://doi.org/10.1021/cs401013v.

[8] P.-P. Knops-Gerrits, D. De Vos, F. Thibault-Starzyk, P. Jacobs, Zeolite-encapsulated Mn(II) complexes as catalysts for selective alkene oxidation, Nature 365 (1994) 543–546, https://doi.org/10.1038/369543a0.

[9] A.P. Wight, M.E. Davis, Design and preparation of organic-inorganic hybrid catalysts, Chem. Rev. 102 (2002) 3589–3614, https://doi.org/10.1021/cr010334m.

[10] P.Q. Liao, J.Q. Shen, J.P. Zhang, Metal–organic frameworks for electrocatalysis, Coord. Chem. Rev. 373 (2018) 22–48, https://doi.org/10.1016/j.ccr.2017.09.001.

[11] Y. Ge, Z. Lyu, M. Marcos-Hernández, D. Villagrán, Free-base porphyrin polymer for bifunctional electrochemical water splitting, Chem. Sci. 13 (2022) 8597–8604, https://doi.org/10.1039/d2sc01250b.

[12] C. Strietzel, M. Sterby, H. Huang, M. Strømme, R. Emanuelsson, M. Sjödin, An aqueous conducting redox-polymer-based proton battery that can withstand rapid constant-voltage charging and sub-zero temperatures, Angew. Chem. Int. Ed. 59 (2020) 9631–9638, https://doi.org/10.1002/anie.202001191.

[13] H. Wang, R. Emanuelsson, H. Liu, K. Edström, F. Mamedov, M. Strømme, M. Sjödin, Redox-state-dependent interplay between pendant group and conducting polymer backbone in quinone-based conducting redox polymers for lithium ion batteries, ACS Appl. Energy Mater. (2019), https://doi.org/10.1021/acsaem.9b01130.

[14] M. Sterby, R. Emanuelsson, F. Mamedov, M. Strømme, M. Sjödin, Investigating electron transport in a PEDOT/Quinone conducting redox polymer with in situ methods, Electrochim. Acta 308 (2019) 277–284, https://doi.org/10.1016/j.electacta.2019.03.207.

[15] F. Zaar, S. Olsson, R. Emanuelsson, M. Strømme, M. Sjödin, Characterization of a porphyrin-functionalized conducting polymer: a first step towards sustainable electrocatalysis, Electrochim. Acta 424 (2022), https://doi.org/10.1016/j.electacta.2022.140616.

[16] S. Watpathomsub, J. Luangchaiyaporn, N.S. Sariciftci, P. Thamyongkit, Efficient heterogeneous catalysis by pendant metalloporphyrin-functionalized polythiophenes for the electrochemical reduction of carbon dioxide, New J. Chem. 44 (2020) 12486–12495, https://doi.org/10.1039/D0NJ01381A.

[17] D. Konev, O. Istakova, B. Dembinska, M. Skunik-Nuckowska, C. Devillers, O. Heintz, P. Kulesza, M. Vorotyntsev, Electrocatalytic properties of manganese and cobalt polyporphine films toward oxygen reduction reaction, J. Electroanal. Chem. 816 (2018) 83–91, https://doi.org/10.1016/j.jelechem.2018.03.042.

[18] A. Nantalaksakul, K. Krishnamoorthy, S. Thayumanavan, Broadening absorption in conductive polymers through cross-linkable side chains in a nonconjugated polymer backbone, Macromolecules 43 (2009) 37–43, https://doi.org/10.1021/ma901850z.

[19] A. Kütt, S. Tshepelevitsh, J. Saame, M. Lõkov, I. Kaljurand, S. Selberg, I. Leito, Strengths of acids in acetonitrile, Eur. J. Org. Chem. 2021 (2021) 1407–1419, https://doi.org/10.1002/ejoc.202001649.

[20] A. Kütt, T. Rodima, J. Saame, E. Raamat, V. Mäemets, I. Kaljurand, I.A. Koppel, R. Y. Garlyauskayte, Y.L. Yagupolskii, L.M. Yagupolskii, E. Bernhardt, H. Willner, I. Leito, Equilibrium acidities of superacids, J. Org. Chem. 76 (2011) 391–395, https://doi.org/10.1021/jo101409p.

[21] D.V. Konev, O.I. Istakova, B. Dembinska, M. Skunik-Nuckowska, C.H. Devillers, O. Heintz, P.J. Kulesza, M.A. Vorotyntsev, Electrocatalytic properties of manganese and cobalt polyporphine films toward oxygen reduction reaction, J. Electroanal. Chem. 816 (2018) 83–91, https://doi.org/10.1016/j.jelechem.2018.03.042.

[22] J. Heinze, B. Frontana-Uribe, S. Ludwigs, Electrochemistry of conducting polymers – persistent models and new concepts, Chem. Rev. 110 (2010) 4724–4771, https://doi.org/10.1021/cr900226k.

[23] M. Wieland, C. Malacrida, Q. Yu, C. Schlewitz, L. Scapinello, A. Penoni, S. Ludwigs, Conductance and spectroscopic mapping of EDOT polymer films upon electrochemical doping, Flex. Print. 5 (2020), 014016, https://doi.org/10.1088/2058-8585/ab76e0.

[24] A. Stanienda, G. Biebl, Elektrochemische untersuchungen an porphinen, Z. Phys. Chem. 52 (1967) 254–275, https://doi.org/10.1524/zpch.1967.52.5_6.254.

[25] R. Felton, H. Linschitz, Polarographic reduction of porphyrins and electron spin resonance of porphyrin anions, J. Am. Chem. Soc. 88 (1966) 1113–1116, https://doi.org/10.1021/ja00958a004.

[26] L. Ye, Y. Fang, Z. Ou, S. Xue, K. Kadish, Cobalt tetrabutano- and tetrabenzotetraarylporphyrin complexes: effect of substituents on the electrochemical properties and catalytic activity of oxygen reduction reactions, Inorg. Chem. 56 (2017) 13613–13626, https://doi.org/10.1021/acs.inorgchem.7b02405.

[27] A. Wolberg, Redox properties of tetraphenylporphyrin complexes, Isr. J. Chem. 12 (1974) 1031–1035, https://doi.org/10.1002/ijch.197400098.

[28] A. Wolberg, J. Manassen, Electrochemical and electron paramagnetic resonance studies of metalloporphyrins and their electrochemical oxidation products, J. Am. Chem. Soc. 92 (1970) 2982–2991, https://doi.org/10.1021/ja00713a010.

[29] A. Giraudeau, H. Callot, J. Jordan, I. Ezhar, M. Gross, Substituent effects in the electroreduction of porphyrins and metalloporphyrins, J. Am. Chem. Soc. 101 (1979) 3857–3862, https://doi.org/10.1021/ja00508a024.

[30] A. Wahab, M. Bhattacharya, S. Ghosh, A. Samuelson, P. Das, Quadratic nonlinearity of one- and two-electron oxidized metalloporphyrins and their switching in solution, J. Phys. Chem. B. 112 (2008) 2842–2847, https://doi.org/10.1021/jp076909m.

[31] L. Truxillo, D. Davis, Electrochemistry of cobalt tetraphenylporphyrin in aprotic media, Anal. Chem. 47 (1975) 2260–2267, https://doi.org/10.1021/ac60363a052.

[32] Y. Fang, F. Mandoj, L. Zeng, R. Pudi, M. Stefanelli, R. Paolesse, K. Kadish, Electrochemistry and spectroelectrochemistry of β-pyrazino-fused tetraarylporphyrins in nonaqueous media, J. Porphyr. Phthalocyanines. 19 (2015) 1–10, https://doi.org/10.1142/S1088424615500224.

[33] A. Giraudeau, H. Callot, M. Gross, Effects of electron-withdrawing substituents on the electrochemical oxidation of porphyrins, Inorg. Chem. 18 (1979) 201–206, https://doi.org/10.1021/ic50191a042.

[34] H. Callat, A. Giraudeau, M. Gross, Cyanoporphyrins. Co-ordinating and electrochemical properties, J. Chem. Soc., Perkin Trans. 2 (1975) 1321–1324, https://doi.org/10.1039/P29750001321.

[35] T. Kohshin, K. Horino, T. Komura, K. Murata, Photovoltaic properties of porphyrin thin films mixed with *o*-chloranil, Bull. Chem. Soc. Jpn. 66 (1993) 733–738, https://doi.org/10.1246/bcsj.66.733.

[36] K. Kadish, L. Shiue, Reactions of metalloporphyrin π radicals. 3. Solvent-and ligand-binding effects on the one-electron oxidation of 5,10,15,20-tetraphenylporphyrin d^{10} metal ions in nonaqueous media, Inorg. Chem. 21 (1982) 3623–3630, https://doi.org/10.1021/ic00140a009.

[37] S. Schmidt, G. Schuster, Anomalous metalloporphyrin and chlorophyll a activated chemiluminescence of dimethyldioxetanone. Chemically initiated electron-exchange luminescence, J. Am. Chem. Soc. 102 (1980) 7100–7103, https://doi.org/10.1021/ja00543a036.

[38] D. Clack, N. Hush, Successive one-electron reduction potentials of porphins and metal porphins in dimethylformamide, J. Am. Chem. Soc. 87 (1965) 4238–4242, https://doi.org/10.1021/ja00947a004.

[39] A. Brown, F. Anson, Cyclic and differential pulse voltammetric behavior of reactants confined to the electrode surface, Anal. Chem. 49 (1977) 1589–1595, https://doi.org/10.1021/ac50019a033.

[40] R. Nicholson, I. Shain, Theory of stationary electrode polarography: single scan and cyclic methods applied to reversible, irreversible, and kinetic systems, Anal. Chem. 36 (1964) 706–723, https://doi.org/10.1021/ac60210a007.

[41] C. Karlsson, H. Huang, M. Strømme, A. Gogoll, M. Sjödin, Ion- and electron transport in pyrrole/quinone conducting redox polymers investigated by in situ conductivity methods, Electrochim. Acta 179 (2015) 336–342, https://doi.org/10.1016/j.electacta.2015.02.193.

[42] I. Bhugun, D. Lexa, J.-M. Savéant, Homogeneous catalysis of electrochemical hydrogen evolution by Iron(0) porphyrin, J. Am. Chem. Soc. 118 (1996) 3982–3983, https://doi.org/10.1021/ja954326x.

[43] A. Maher, G. Passard, D. Dogutan, R. Halbach, B. Anderson, C. Gagliardi, M. Taniguchi, J. Lindsey, D. Nocera, Hydrogen evolution catalysis by a sparsely

substituted cobalt chlorin, ACS Catal. 7 (2017) 3597–3606, https://doi.org/10.1021/acscatal.7b00969.
[44] B. Beyene, S. Mane, C. Hung, Electrochemical hydrogen evolution by cobalt (II) porphyrins: effects of ligand modification on catalytic activity, efficiency and overpotential, J. Electrochem. Soc. 165 (2018) H481–H487, https://doi.org/10.1149/2.0481809jes.
[45] M.L. Pegis, D.J. Martin, C.F. Wise, A.C. Brezny, S.I. Johnson, L.E. Johnson, N. Kumar, S. Raugei, J.M. Mayer, Mechanism of catalytic O2 reduction by iron tetraphenylporphyrin, J. Am. Chem. Soc. 141 (2020) 8315–8326, https://doi.org/10.1021/jacs.9b02640.
[46] R. Zhang, J.J. Warren, Controlling the oxygen reduction selectivity of asymmetric cobalt porphyrins by using local electrostatic interactions, J. Am. Chem. Soc. 142 (2020) 13426–13434, https://doi.org/10.1021/jacs.0c03861.
[47] G. Passard, D.K. Dogutan, M. Qiu, C. Costentin, D.G. Nocera, Oxygen reduction reaction promoted by manganese porphyrins, ACS Catal. 8 (2018) 8671–8679, https://doi.org/10.1021/acscatal.8b01944.
[48] C.T. Carver, B.D. Matson, J.M. Mayer, Electrocatalytic oxygen reduction by iron tetra-arylporphyrins bearing pendant proton relays, J. Am. Chem. Soc. 134 (2012) 5444–5447, https://doi.org/10.1021/ja211987f.